GEORGE BROWN PRESS
JOURNALS, BOOKS & PROCEEDINGS

Journal of Computer, Signal, and System Research

Article

From Subjective to Objective: Developing EEG-Based Indicators for Competency Assessment in Low-Altitude Aviation Training

Qing Liu [1,*] and Jiayun Zhang [1]

[1] College of Transportation Science and Engineering, Civil Aviation University of China, Tianjin, China
* Correspondence: Qing Liu, College of Transportation Science and Engineering, Civil Aviation University of China, Tianjin, China

Abstract: The global advancement of the low-altitude economy has led to a significant increase in low-altitude aircraft operations and activities. Consequently, the selection and training of pilots for these aircraft have become focal points in both research and regulatory oversight. Traditional competency assessments often rely on subjective questionnaires, behavioral tests, or simulator training records. While these approaches can reflect macro-level performance, they exhibit limitations in objectivity, real-time capability, and the interpretation of underlying physiological mechanisms. Electroencephalography (EEG), a non-invasive physiological signal with high temporal resolution, offers a promising tool for pilot selection, training, and real-time monitoring of cognitive states. This study develops a resting-state EEG-based indicator to assess pilot competency. We designed a novel paradigm to collect multi-channel resting EEG from 20 participants. After preprocessing, signals were segmented into 4-second epochs. We extracted 14 features including power spectral density, differential entropy, and time-domain variance, analyzed across standard frequency bands. Using balanced samples per participant, we evaluated five classifiers via 10-fold cross-validation, comparing performance across bands, channels, and features. Results indicate that differential entropy features in the gamma band, particularly from the FP1 and P3 channels, demonstrated a significant ability to distinguish pilot competency. Classification accuracy based on single-channel gamma band DE features exceeded 80%. Model performance was further quantified using a confusion matrix and multiple metrics, such as accuracy, precision, recall, and F1-score. The study also discusses limitations related to sample size, model generalizability, and practical engineering applications, along with potential directions for improvement.

Keywords: Trainees; competence; personnel selection; vocational aptitude; aviation education; EEG

Received: 03 March 2026
Revised: 18 April 2026
Accepted: 29 April 2026
Published: 05 May 2026

1. Introduction

The low-altitude economy, constituting a vital segment of general aviation, represents a strategically important sector for China's future economic development [1]. Benefiting from both intensive low-altitude airspace utilization and substantial policy-economic support, this domain is undergoing robust expansion. Low-altitude aviation operations encompass diverse applications including logistics, aerial photography, remote sensing, and transportation services, all facilitated by corresponding aircraft such as unmanned aerial vehicles, manned aircraft, and air taxis [2]. The proliferation of low-altitude aircraft has correspondingly elevated competency requirements for operators. Research indicates that general aviation pilots demonstrate disproportionately higher involvement in aeronautical decision-making incidents compared to commercial pilots [3]. This discrepancy stems from the inherently greater frequency of unexpected scenarios encountered during general aviation operations. Furthermore, low-altitude aircraft operators face particularly challenging flight environments characterized by lower altitudes alongside more complex airspace and terrain configurations, necessitating

enhanced capability for frequent emergency response. Consequently, ensuring the safety of low-altitude flight missions demands rigorous attention to three critical aspects: real-time monitoring of operator cognitive states, refined personnel selection protocols, and systematic training methodologies. These elements collectively form the foundation for sustainable development within this rapidly evolving aviation sector.

Existing research on traditional pilot assessment and selection predominantly relies on psychometric instruments. These subjective measures are vulnerable to response manipulation and are typically administered at discontinuous time points detached from actual operational contexts. By the time of assessment, transient emotional responses have normalized, rendering such evaluations inadequate for capturing dynamic cognitive processes [4]. This situation underscores the critical need for transitioning competency evaluation systems from experience-based judgment toward scientific, quantitative methodologies [3]. Furthermore, conventional studies primarily focus on transient conditions such as workload and fatigue, while largely neglecting the fundamental assessment of core competency. The ability to identify inherent suitability during initial selection phases would enable more precise identification of promising candidates. Consequently, establishing an objective evaluation framework for low-altitude aircraft operator competency becomes imperative, necessitating the adoption of quantifiable physiological indicators to replace subjective measurements.

Given these requirements, electroencephalography has emerged as a suitable methodology due to its non-invasive nature and high temporal resolution. As an established physiological measurement technique, EEG is extensively utilized to characterize task performance, emotional states, and individual capability differences. Accordingly, this research employs EEG signal acquisition combined with machine learning algorithms to identify objective physiological indicators capable of distinguishing operator competency in low-altitude aircraft operations. Existing literature demonstrates the successful application of EEG metrics as quantitative assessment tools across various professional domains, including automotive drivers, commercial aviation pilots, competitive athletes, and clinical populations with depressive disorders.

Building upon existing research, Sharif et al. demonstrated that low-alpha band (8-10 Hz) activity serves as a key biomarker for distinguishing expert neurosurgeons from novices through EEG analysis and seven machine learning models, establishing EEG's validity for precise surgical skill quantification [5]. In educational settings, Fuentes-Martinez et al. collected EEG signals from secondary students to evaluate attention levels and academic performance, revealing significant correlations between beta-band power spectral density and learning outcomes [6].

Transportation safety research shows parallel advancements. Aminosharieh et al. developed multimodal assessment frameworks integrating EEG, electrocardiogram (ECG), and electrodermal activity (EDA) to monitor driver attention during simulated operations [7]. Similarly, Angkan et al. demonstrated that EEG combined with wearable sensors can accurately measure cognitive load in vehicular operation contexts [8].

Extending to aviation physiology, Asaf et al. acquired EEG recordings from Israeli Air Force flight cadets and UAV operators under sleep deprivation conditions. By applying machine learning algorithms, they achieved high-precision prediction of psychomotor vigilance task performance, while additionally examining the importance of different EEG features and their contribution to changes in the behavioral metrics [9]. Hu et al. further validated the correlation between EEG characteristics from the C3 and C4 regions and anti-vertigo tolerance in civil aviation flight students [10]. These findings collectively provide a theoretical foundation for the present study, while demonstrating the broader applicability of neural markers in aviation personnel assessment.

This study focuses on identifying objective physiological indicators for assessing low-altitude aircraft operator competency. It innovatively integrates resting-state EEG characteristics with operational performance evaluation through an experimental paradigm incorporating both positive and negative emotional stimuli. During the experiments, continuous EEG recordings were obtained to systematically explore the

relationship between 14 neural features across five frequency bands and operational competency. The results revealed statistically significant gamma-band spectral features in the FP1 and P3 channels, with subsequent analysis examining the potential neurophysiological mechanisms underlying this observation. These findings provide empirical support for developing competency assessment tools while suggesting practical modifications to training curricula, particularly through the integration of targeted cognitive modules. The study offers valuable insights for cultivating professional talent within the global low-altitude economy sector.

2. Experimental Design

2.1. Participants

The study recruited 20 participants from the Civil Aviation University of China, all students from the College of Transportation Science and Engineering. The cohort comprised 10 undergraduate students majoring in Unmanned Aircraft Systems and 10 graduate students specializing in General Aviation Management and Technology. The sample included 7 females and 13 males, aged 20-25 years. All participants had received professional theoretical training and were preparing for the Civil Aviation Administration of China (CAAC) Unmanned Aircraft Operator License examination.

Selection criteria required all subjects to be in good health with no history of cephalic trauma. Prior to the experiment, participants followed strict protocols: they abstained from caffeine and alcohol consumption for 12 hours, avoided any psychoactive medications, refrained from strenuous exercise, and maintained smoking abstinence. Within the final hour before testing, subjects avoided cold food intake and vigorous physical activity while reporting no subjective discomfort. During EEG recordings, all metallic accessories and eyeglasses were removed to ensure signal quality.

2.2. Materials and Equipment

The experimental stimuli consisted of video materials selected based on established methodological frameworks. A 150-second clip from "Pegasus 2" served as the positive emotional inducer, while a 150-second segment from "Aftershock" was utilized for negative emotional provocation. The experiment was conducted in an acoustically isolated and well-lit laboratory setting.

Physiological signals were acquired using a Greentek 11-channel non-invasive EEG electrode cap (Model BM-LA01-2011). The collected data were transmitted through a Nuo Cheng EEG amplifier (Z2N-F-20-C) and wireless Bluetooth receiver (Z2N-JS-USB-3) to Shanghai Nuo Cheng's NCERP software. Exported data were subsequently processed in MATLAB and EEGLAB environments for analysis. All physiological signals were sampled at 128 Hz with electrode placement conforming to the international 10-20 system.

2.3. Experimental Paradigm Design

The use of emotional induction materials, such as videos with positive and negative emotional valence, represents a well-established methodology for eliciting distinct psychological states and observing corresponding EEG responses. To ensure reproducible elicitation effects and signal quality, standard protocols typically include: resting baseline measurements, multiple short-duration induction segments, and interleaved rest periods, supplemented by pre- and post-experiment questionnaires for subjective labeling and validation. The present study strictly adheres to this established paradigm while implementing specific modifications and enhancements.

All participants initially completed an informed consent form and basic information questionnaire, acknowledging that their data would be utilized for master's degree research at Civil Aviation University of China. The experimental procedures were thoroughly explained beforehand. Each subject underwent a single data collection session following the standardized protocol, with physiological signals from all 20 participants acquired over a three-day period. The complete experimental procedure was designed to conclude within 25 minutes.

The protocol commenced with a 5-minute closed-eye resting-state EEG recording. Following a 2-minute rest period, participants underwent a 3-minute positive video stimulus segment with concurrent EEG acquisition. After another 2-minute interval, a 3-minute negative video stimulus was presented during EEG recording (Table 1). Upon completion, subjects filled out a competency assessment scale to conclude the experimental session.

Table 1. Experimental Procedures and Instructions.

experimental procedure	Explain	time /min
1.Experimental Introduction and Preparation	Briefly explain the experimental procedure to the participants and have them wear the electrode caps to properly set up the data collection equipment.	5
2.Resting experiment	Eye-closed rest experiment	5
3.Rest	Calm down and get ready to proceed to the next experiment	2
4.positive video experiment	The positive induction materials are divided into 4 periods, totaling 180 seconds. The first 5 seconds are for prompting the participants to pay attention, during which the participants remain at rest. The next 5 seconds are for the screen to display a prompt that the experiment is about to begin. From 10 seconds to 160 seconds, the corresponding induction materials are played. After the materials are played, the participants have 20 seconds to adjust themselves and calm down, and then the experiment is concluded.	3
5.Rest	Calm down and get ready to proceed to the next experiment	2
6.negative video experiment	The negative induction materials are divided into 4 periods, totaling 180 seconds. The first 5 seconds are for prompting the participants to pay attention, during which the participants remain at rest. The next 5 seconds are for the screen to display a prompt that the experiment is about to begin. From 10 seconds to 160 seconds, the corresponding induction materials are played. After the materials are played, the participants have 20 seconds to adjust themselves and calm down, and then the experiment is concluded.	3
7.scale	Fill in the other scales related to personal information and competency assessment	5

3. Data Processing and Classification Analysis

The study acquired EEG signals from 20 students in the General Aviation Department under three conditions: resting state, positive emotional state, and negative emotional state. The raw data contained substantial noise components, including

electrooculographic artifacts (EOG) from eyelid and eyeball movements, electromyographic artifacts (EMG) from facial muscle contractions or orofacial movements, and electrocardiographic artifacts (ECG) from cardiac activity. Additionally, electromagnetic interference in the experimental environment contributed to signal contamination. Since these artifacts adversely affect subsequent feature extraction and classification, we implemented comprehensive preprocessing procedures to eliminate irrelevant noise components from the acquired EEG signals.

In this experiment, EEG signals were preprocessed using the EEGLAB toolbox, following these sequential steps:

Channel localization and sampling rate configuration. Following data import, electrode positions were standardized. The electrode cap provided eight detectable channels: FP1, FP2, P3, P4, O1, O2, T3, and T4, with a confirmed sampling rate of 128 Hz (Figure 1).

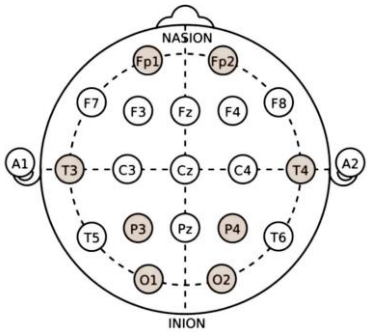

Figure 1. Schematic diagram of 8-channel EEG leads.

Filtering. Band-pass filtering was applied with cutoff frequencies of 0.5 Hz (high-pass) and 40 Hz (low-pass).

Trimming. To eliminate artifacts from initial electrode instability, subject preparation movements, and transient disturbances during start/end periods, the first 10 seconds and final 10 seconds of recording were removed. This retained only the stable, minimally-contaminated EEG segments. After trimming, valid data durations were 280 seconds per subject for Condition A, and 160 seconds each for Conditions B and C. For subsequent feature calculation and statistical analysis, the continuous signals were segmented into non-overlapping 4-second epochs. Each 4-second epoch was treated as an independent sample for feature extraction and classification, optimally covering the five targeted frequency bands while maintaining adequate temporal resolution.

Rereferencing: The data were rereferenced to the average of all channels using EEGLAB's standard procedure.

Independent Component Analysis (ICA): ICA was employed to decompose the EEG signals into statistically independent components. Components identified as ocular or muscular artifacts were removed using EEGLAB in conjunction with the ICLabel plugin, thereby minimizing their impact on subsequent analysis.

Following preprocessing, 14 distinct features were extracted from each channel: Power Spectral Density (PSD), Differential Entropy (DE), Mean, Variance, Kurtosis, Skewness, Zero-crossing Rate, Hjorth Activity (HA), Hjorth Mobility (HM), Hjorth Complexity (HC), Sample Entropy (SE), Fractal Dimension (FD), Permutation Lempel-Ziv Complexity (PLZC), and Wavelet Entropy (WE). These features were systematically numbered for subsequent analysis.

3.1. Power Spectral Density

Power Spectral Density (PSD) quantifies the signal's power distribution in the frequency domain, reflecting the energy intensity across five frequency bands: Delta, Theta, Alpha, Beta, and Gamma. In resting-state EEG analysis, Power Spectral Density directly represents spectral power variations between different bands, facilitating the

generation of frequency-band topographic maps and enabling band-specific classification. The computational procedure is described as follows:

The discrete-time signal is segmented into multiple overlapping shorter epochs. Each epoch is windowed, and its periodogram is computed. Welch's Power Spectral Density estimate is obtained by averaging these periodograms across all segments. Subsequently, band power for specific frequency bands of interest is calculated through spectral integration of the Power Spectral Density over the corresponding frequency ranges.

Step 1: Windowed DFT for a Single Segment (r-th segment)

For the r-th segment of length L, given a window function w(n), its Discrete Fourier Transform is calculated as follows:

$X_r(k) = \sum_{n=0}^{L-1} w[n] \quad x[n + rD] e^{-j2\pi kn/N_{\text{fft}}}$

where D represents the hop size and Nfft denotes the number of transformation points [11].

Step 2: Modified Periodogram (Segment Power Spectrum)

Normalized by the window energy $U = \sum_{n=0}^{L-1} w[n]^2$, the power spectrum of the r-th segment is given by:

$$P_r(f_k) = \frac{1}{U} |X_r(k)|^2 \quad (2)$$

Step 3: Welch Power Spectral Density

$$\bar{S}_x(f_k) = \frac{1}{K} \sum_{r=0}^{K-1} P_r(f_k) = \frac{1}{KU} \sum_{r=0}^{K-1} |X_r(k)|^2 \quad (3)$$

This $\bar{S}_x(f_k)$ represents the power spectral density estimate at f_k (unit: signal squared per Hz) [12].

Step 4: band power

The total power within frequency band $[f_a, f_b]$ is obtained by integrating the Power Spectral Density over this band [13].

$$P_{band} = \int_{f_a}^{f_b} \bar{S}_x(f) df \quad (4)$$

At discrete frequency points, this operation is equivalently computed as the summation of $\bar{S}_x(f_k)$ across the band, multiplied by the frequency resolution Δf .

Step 5: Relative Power

Relative power is actually also normalized. To mitigate the effects of inter-individual variations in total signal power, the relative band power is commonly employed:

$$Rel\ \text{Power}_{\text{band}} = \frac{P_{band}}{\sum_{f_{min}}^{f_{max}} \bar{S}_x(f) \Delta f} \quad (5)$$

The denominator may be defined as the total power across the entire analysis band.

Symbol Description:

$x[n]$: Discrete-time EEG signal sample

f_s: Sampling frequency

L: Window length per segment

D: hop size

$w[n]$: Window function

$U = \sum w(n)^2$: Window energy normalization constant

K: Number of segments (total obtainable short-time epochs)

N_{fft}: Number of FFT points (determining frequency resolution)

$\bar{S}_x(f)$: Welch PSD estimate

P_{band} , $Rel\ \text{Power}_{\text{band}}$:Absolute and relative band power

3.2. Differential Entropy

Differential Entropy (DE) extends the concept of entropy to continuous random variables, serving to quantify the uncertainty within a signal segment. Under Gaussian approximation, it possesses an analytical relationship with the signal variance within the segment. In research applications, Differential Entropy transforms energy information into a logarithmic scale, often demonstrating greater stability and reduced sensitivity to amplitude scaling compared to raw power metrics. This property makes it suitable as a supplementary or alternative feature for classification tasks, enhancing classifier

robustness against inter-subject amplitude variability [14]. For a real-valued random variable $X \sim N(\mu, \sigma^2)$ that satisfies the Gaussian distribution assumption, its differential entropy is given by the following analytical expression:

$$h(X) = \frac{1}{2} ln(2\pi e\sigma^2) \quad (6)$$

In this equation, a represents the variance of X, and ln denotes the natural logarithm. The resulting value is expressed in nats [15].

In EEG signal processing, the implementation procedure adopted in this study involves:

Step 1: Band-pass Filtering for Frequency Separation

The raw EEG or segmented temporal signals are first band-pass filtered into targeted frequency bands (e.g. $\delta, \theta, \alpha, \beta, \gamma$), yielding band-specific temporal signals for subsequent analysis [16].

Step 2: Epoch Segmentation

The filtered temporal signals are divided into fixed-duration epochs to ensure statistical stationarity within each segment. This study employs 4-second epochs for this purpose.

Step 3: Mean Removal

The mean value of each segment is subtracted to achieve zero-centering, ensuring the subsequent variance estimation remains unaffected by DC components.

Step 4: Variance Estimation

The variance $\hat{\sigma}^2$ is computed from the samples within the zero-centered segment.

Step 5: Differential Entropy Calculation

Under the Gaussian assumption, the differential entropy is calculated by substituting the estimated variance into its analytical expression:

$$DE = \frac{1}{2} ln(2\pi e\hat{\sigma}^2) \quad (7)$$

Step 6: Feature Organization

The calculated Differential Entropy values from each epoch, channel, and frequency band serve as input features for subsequent statistical testing and classifier training. For the temporal signal of each channel and frequency band, we first segment the data into non-overlapping 4-second epochs. Each epoch undergoes mean removal followed by computation of the sample variance [16].

3.3. Variance

Variance, defined as the sample variance within a signal segment, quantifies the temporal domain energy and fluctuation amplitude of the signal, reflecting the dispersion of potential amplitudes. In resting-state EEG analysis, variance serves as one of the most fundamental and widely used temporal features for characterizing signal energy and intensity in short-term epochs. However, it exhibits high sensitivity to high-amplitude artifacts such as ocular or muscle activity. Therefore, its application for statistical comparisons or classifier input requires rigorous artifact removal and within-segment normalization.

For each channel and frequency band, after identical preprocessing steps, consider a single epoch $x(n)$ containing N sample points with sample values denoted as $\{x[1], x[2], \ldots, x[N]\}$. The variance is computed as follows:

Step 1: Segment Mean (Sample Mean)

$$\bar{x} = \frac{1}{N} \sum_{n=1}^{N} x[n] \quad (8)$$

Step 2: Sample Variance

$$\hat{\sigma}^2 = \frac{1}{N} \sum_{n=1}^{N} (x[n] - \bar{x})^2 \quad (9)$$

Step 3: Feature Organization

The $\hat{\sigma}^2$ value from each epoch, channel, and frequency band is utilized as the Variance feature. To enhance numerical stability, logarithmic transformation or z-score normalization of the variance may be applied prior to statistical testing or classifier input. For the temporal signal of each channel, this study first segmented the data into non-

overlapping 4-second epochs, followed by mean removal within each epoch. For the i-th signal segment $x_i[n]$ (containing N sample points), the sample variance is computed as the feature:

$$VAR_i = \hat{\sigma}^2 = \frac{1}{N}\sum_{n=1}^{N}(x[n] - \bar{x})^2 \quad (10)$$

The variance values from all segments (across epochs×channels×frequency bands) form the feature matrix, which serves as the foundation for subsequent statistical testing and classification. To mitigate the effects of scale differences and inter-subject variability, z-score standardization was applied to each feature dimension using the training set parameters before classification, with these same parameters subsequently applied to the testing set.

3.4. Model Selection and Evaluation

This study employed five common binary classification methods to evaluate the discriminative capacity of EEG features for subject competency status. The selected baseline models include: (1) K-Nearest Neighbors (KNN), a non-parametric method utilizing local neighborhood similarity in the sample space, suitable for proximity-based classification without strong distributional assumptions; (2) Random Forest (RF), an ensemble learning method based on decision trees that enhances stability through majority voting while inherently handling non-linear relationships and feature interactions; (3) Support Vector Machine (SVM), a discriminant classifier based on margin maximization that constructs robust separation boundaries in high-dimensional feature spaces; (4) Naive Bayes (NB), a probabilistic model employing conditional independence assumptions, computationally efficient and commonly used for rapid baseline comparisons; (5) Logistic Regression (LR), a linear probability model providing direct class probability estimates, facilitating threshold adjustment and interpretability.

All methods were evaluated under consistent normalization and cross-validation frameworks within the same fold. Performance was assessed using fundamental binary classification metrics derived from the confusion matrix-including Accuracy, Precision, Recall, and F1-score-as primary evaluation parameters (Figure 2). In this binary classification task, label "1" was defined as the positive class (i.e., "competent"), while label "0" was designated as the negative class (i.e., "not competent"). To intuitively visualize the classifier's prediction distribution across true classes, the confusion matrices in this study are presented in row-normalized percentage format. The fundamental concept of the confusion matrix calculation is outlined as follows:

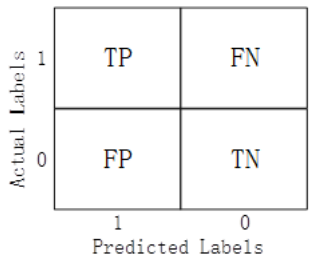

Figure 2. Confusion matrix.

True Positive (TP) refers to the number of samples correctly predicted as "competent" when the actual label is "competent".

False Positive (FP) denotes the number of samples incorrectly predicted as "competent" when the actual label is "not competent".

False Negative (FN) represents the number of samples incorrectly predicted as "not competent" when the actual label is "competent".

True Negative (TN) indicates the number of samples correctly predicted as "not competent" when the actual label is "not competent".

Accuracy measures the proportion of correctly predicted samples among the total samples, calculated as:

$$Accuracy=\frac{TP+TN}{TP+TN+FN+FP} \quad (11)$$

Recall measures the proportion of actual positive cases ("competent") that are correctly identified, calculated as:

$$Recall=\frac{TP}{TP+FN} \quad (12)$$

Precision quantifies the proportion of samples correctly predicted as "competent" among all samples predicted as "competent", calculated as:

$$Pr\,e\,\text{scision}=\frac{TP}{TP+FP} \quad (13)$$

The F1-score represents the harmonic mean of recall and precision, calculated using the formula:

$$F_1=2\frac{Pr\,e\text{cision}\times\text{Recall}}{Pr\,e\text{cision}+\text{Recall}} \quad (14)$$

False Positive Rate (FPR) represents the proportion of samples incorrectly identified as "competent" among all truly "not competent" samples. Its value range is [0,1].

$$FPR=\frac{FP}{FP+TN} \quad (15)$$

False Negative Rate (FNR) represents the proportion of samples incorrectly predicted as "not competent" among all truly "competent" samples. Its value range is [0, 1].

$$FNR=\frac{FN}{TP+FN}=1-Recall \quad (16)$$

4. Results

The experimental investigation employed a novel paradigm to collect electroencephalographic (EEG) data from low-altitude aircraft operators. A total of 14 distinct EEG features were extracted and evaluated using five classification algorithms: K-Nearest Neighbors (KNN), Random Forest (RF), Support Vector Machine (SVM), Naive Bayes (NB), and Logistic Regression (LR). Comparative analysis of classification accuracy, as summarized in Table 2, Table 3 and Table 4 identified the combination of Power Spectral Density (PSD), Differential Entropy (DE), and Variance (VAR) features with the KNN classifier as the optimal configuration. This specific feature set and classifier pairing demonstrated superior predictive performance in distinguishing operator competency levels.

Table 2. Classifier Performance Analysis: Results from Dataset A.

	Classifier	Delta	Theta	Alpha	Beta	Gamma	Mean
PSD	SVM	66.5000	63.0000	70.5000	83.7500	84.7500	73.7000
	KNN	83.2500	73.7500	87.5000	92.2500	97.3750	86.8250
	RF	79.3750	73.6250	83.8750	89.1250	95.7500	84.3500
	NB	64.3750	56.2500	65.2500	76.7500	76.2500	67.7750
	LR	65.2500	61.1250	69.5000	83.1250	84.8750	72.7750
DE	SVM	60.0000	66.5000	63.8750	60.0000	64.6250	63.0000
	KNN	77.2500	72.2500	78.0000	63.6250	63.2500	70.8750
	RF	74.5000	69.5000	73.5000	59.5000	60.8750	67.5750
	NB	56.5000	64.7500	61.8750	63.7500	63.7500	62.1250
	LR	62.5000	65.6250	63.8750	63.5000	64.3750	63.9750
VAR	SVM	60.0000	60.0000	59.7500	60.0000	60.0000	59.9500
	KNN	75.1250	71.8750	75.1250	63.3750	63.2500	69.7500
	RF	74.5000	69.6250	73.1250	59.5000	61.0000	67.5500
	NB	58.8750	43.8750	58.2500	60.2500	59.7500	56.2000
	LR	61.0000	59.3750	59.7500	60.0000	60.7500	60.1750

Table 3. Classifier Performance Analysis: Results from Dataset B.

	Classifier	Delta	Theta	Alpha	Beta	Gamma	Mean

	SVM	64.7500	70.8750	61.6250	74.5000	75.1250	69.3750
	KNN	83.6250	76.5000	71.2500	89.2500	94.5000	83.0250
PSD	RF	84.0000	77.3750	70.8750	88.0000	92.7500	82.6000
	NB	63.8750	61.5000	57.2500	62.6250	54.6250	59.9750
	LR	64.2500	70.8750	61.8750	73.6250	75.0000	69.1250
	SVM	78.5000	76.0000	69.2500	60.0000	71.7500	71.1000
	KNN	84.1250	90.3750	71.5000	54.2500	65.3750	73.1250
DE	RF	82.2500	89.8750	70.1250	53.6250	61.2500	71.4250
	NB	70.3750	69.3750	64.8750	58.8750	72.1250	67.1250
	LR	78.0000	72.3750	67.2500	57.2500	72.0000	69.3750
	SVM	60.0000	60.0000	60.0000	60.0000	67.3750	61.4750
	KNN	84.7500	88.2500	70.0000	54.5000	65.7500	72.6500
VAR	RF	82.1250	89.6250	70.2500	53.6250	61.3750	71.4000
	NB	51.0000	57.1250	40.0000	39.8750	45.0000	46.6000
	LR	62.7500	59.5000	60.0000	60.0000	71.1250	62.6750

Table 4. Classifier Performance Analysis: Results from Dataset C.

	Classifier	**Delta**	**Theta**	**Alpha**	**Beta**	**Gamma**	**Mean**
	SVM	71.6756	77.7025	64.4114	75.9351	80.5870	74.0623
	KNN	88.4684	77.5759	73.5617	95.3576	96.3655	86.2658
PSD	RF	86.4684	78.7104	75.3133	93.0949	95.8639	85.8902
	NB	56.5253	71.2943	62.5316	66.0427	63.4288	63.9646
	LR	70.5522	76.8275	63.6614	74.8070	80.3402	73.2377
	SVM	65.2880	57.7516	61.3813	59.0364	74.6899	63.6294
	KNN	84.3291	87.5807	80.0680	65.6598	73.9335	78.3142
DE	RF	82.8212	85.9557	73.7991	60.2816	68.6677	74.3051
	NB	66.5522	66.7611	67.1487	59.0316	76.3180	67.1623
	LR	67.6598	58.6203	60.5032	59.0332	76.3165	64.4266
	SVM	60.7848	66.7706	65.5190	60.1519	66.9193	64.0291
	KNN	82.5744	84.8386	77.4383	65.6598	73.9335	76.8889
VAR	RF	82.8212	85.9557	74.0491	60.1551	68.6677	74.3297
	NB	54.3940	66.5222	63.5174	60.7864	65.2864	62.1013
	LR	67.6646	59.8766	65.1440	58.4066	71.0506	64.4285

Experimental results demonstrate that features exhibiting statistically significant discriminatory power achieved remarkable classification performance through the KNN algorithm, with mean accuracy rates reaching 95% or higher. This outstanding performance established KNN as the primary classifier for subsequent analytical phases. Furthermore, comparative analysis across frequency bands revealed that both beta and gamma bands consistently outperformed the other three frequency bands in classification accuracy. Based on these findings, we generated topographic maps for Power Spectral Density (PSD), Differential Entropy (DE), and Variance (VAR) features within the beta and gamma bands across all three experimental groups (Figure 3, Figure 4, Figure 5). The visualization scheme systematically presents beta-band topographic distributions in the first row, while the first column exclusively displays data from subjects labeled as competent.

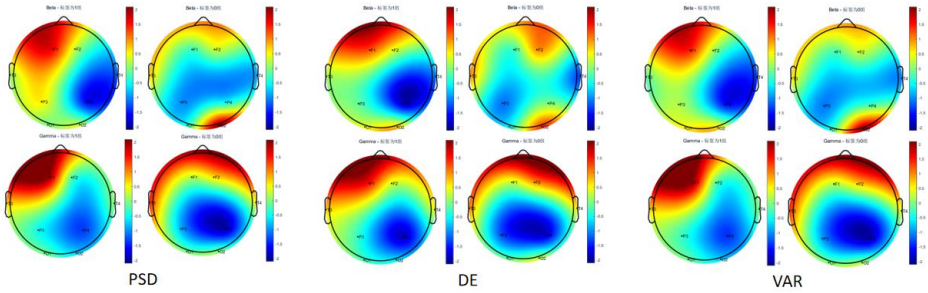

Figure 3. Brain topographic maps of the beta and gamma frequency bands for PSD, DE and VAR features in Group A.

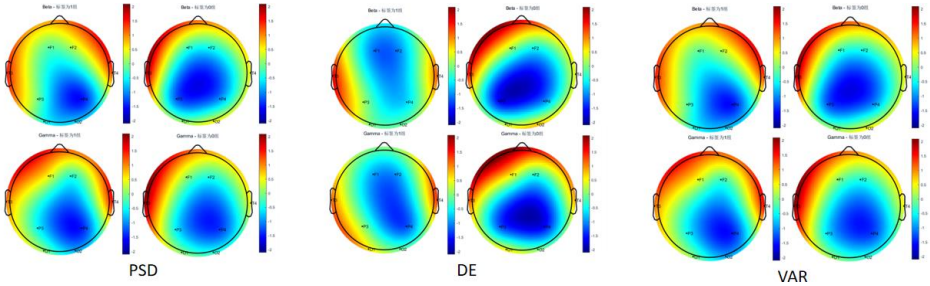

Figure 4. Brain topographic maps of the beta and gamma frequency bands for PSD, DE and VAR features in Group B.

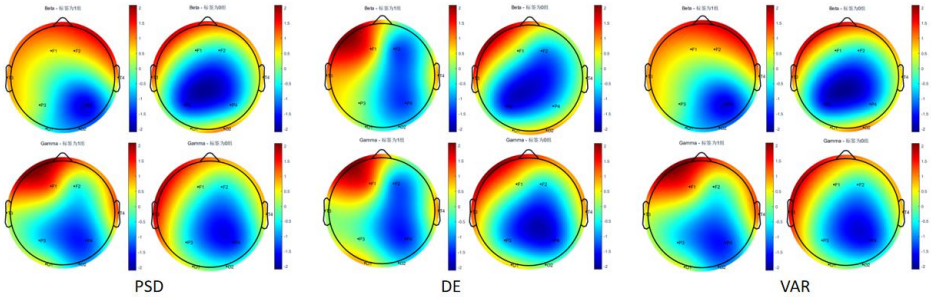

Figure 5. Brain topographic maps of the beta and gamma frequency bands for PSD, DE and VAR features in Group C.

The topographic maps reveal distinct spatial distribution patterns across all three experimental groups in both beta and gamma frequency bands. Subjects labeled as competent consistently demonstrated prominent energy disparities specifically at channels FP1, P3, and O2.

For Group A in the beta frequency band, the Power Spectral Density (PSD) feature demonstrated statistically significant disparities at channels FP1, P3, and O2. The Differential Entropy (DE) feature exhibited notable variations across multiple channels including FP1, P3, P4, O1, O2, and T3. Meanwhile, the Variance (VAR) feature showed significant differentiation at channels FP1, P3, P4, and O2. In the gamma frequency band analysis of Group A, the Power Spectral Density (PSD) feature displayed marked differences primarily at FP1. The Differential Entropy (DE) feature revealed significant variations at both FP1 and P3, while the Variance (VAR) feature demonstrated similar significant differentiations at these two channels.

Further analysis of Groups B and C also revealed substantial inter-group differences with statistically significant channels, which have been systematically compiled in the subsequent table (Table 5) for comprehensive comparison.

Table 5. Statistically Significant Channels for Three Feature Types Across Experimental Groups and Frequency Bands.

Groups	Bands	Feature	Significant Channels
A	Beta	PSD	FP1,P3,O2
A	Beta	DE	FP1,P3,P4,O1,O2,T3
A	Beta	VAR	FP1,P3,P4,O2
A	Gamma	PSD	FP1
A	Gamma	DE	FP1,P3
A	Gamma	VAR	FP1,P3
B	Beta	PSD	P3,T4,O2
B	Beta	DE	FP1,P3,O2
B	Beta	VAR	P3,T4,O2
B	Gamma	PSD	T3,T4,O2
B	Gamma	DE	FP1,P3
B	Gamma	VAR	T3,T4
C	Beta	PSD	FP1,FP2,P3,O2
C	Beta	DE	FP1,P3,O2
C	Beta	VAR	FP1,FP2,P3,O2
C	Gamma	PSD	FP1,T3
C	Gamma	DE	FP1,P3,T3
C	Gamma	VAR	FP1,T3

Analysis of statistically significant channels reveals that FP1 and P3 consistently demonstrate the highest frequency of occurrence across experimental conditions. The competent group, designated as label 1, exhibits significantly higher neural activity at both FP1 and P3 channels compared to the non-competent group.

The FP1 channel corresponds to the prefrontal cortex region, which serves as the physiological foundation for advanced cognitive functions. This brain region primarily engages in complex psychological processes including working memory encoding, motor planning, decision-making, and emotional-behavioral regulation. In the context of low-altitude aircraft operation, these neural mechanisms directly support critical competencies such as flight strategy formulation, attention resource allocation, and behavioral control.

For competency assessment in low-altitude aircraft operators, these cognitive capabilities manifest through sustained high-intensity attention for monitoring multidimensional information streams, real-time decision-making for optimal flight path planning, and effective emotional regulation when confronting unexpected situational pressures [17].

The P3 channel is located in the parietal lobe, recognized as the primary sensory integration center. This region facilitates spatial information processing including navigation and positioning, attention regulation encompassing vigilance maintenance, rapid threat response capability, and fundamental multisensory integration supporting complex task management [18]. As a crucial hub within the attention network, it integrates sensory inputs with spatial information to support operational performance [19].

In evaluating low-altitude aircraft operator competency, this neural substrate correlates strongly with multimodal information integration capacity, high-precision spatial orientation skills, and rapid stress response capabilities. The synergistic integration of these neural functions constitutes the fundamental safeguard for ensuring operational safety within complex low-altitude airspace environments [20].

Confusion matrices were constructed for both beta and gamma frequency bands across all three experimental datasets, with comprehensive performance metrics calculated including accuracy, recall, precision, F1-score, false positive rate, and false negative rate. The clinical implications of misclassification warrant careful consideration:

when the model incorrectly classifies non-competent subjects as competent (false positives), it creates potential safety hazards by granting qualifications to unqualified individuals. Conversely, misclassifying competent subjects as non-competent (false negatives) leads to unnecessary resource allocation and increased training costs.

A decline in precision directly indicates an elevated proportion of subjects being erroneously certified as competent by the system, representing an escalation of potential safety risks. Similarly, a decrease in recall signifies that a substantial number of truly competent subjects are incorrectly rejected, resulting in increased training expenditures and administrative burdens. During model selection, sole optimization of accuracy often fails to capture the critical trade-off between these two types of operational costs. Consequently, the standard practice involves utilizing combined metrics such as the F1-score, which harmonizes precision and recall, or strategically adjusting classification thresholds to balance safety concerns against resource utilization.

The accompanying figure presents confusion matrices for three distinct features within the gamma frequency band of Dataset A, all based on the KNN classifier (Figure 6). Additionally, the subsequent table (Table 6) provides comprehensive computational results derived from confusion matrix analysis across all three experimental datasets, focusing specifically on significant features within their respective predominant frequency bands.

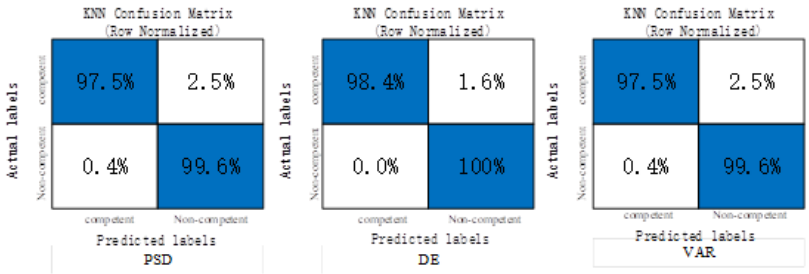

Figure 6. Row-Normalized Confusion Matrices for PSD, DE, and VAR Features in the Gamma Band (Dataset A).

Table 6. Computational Results of Confusion Matrices for Significant Features and Frequency Bands.

Groups	Features and Bands	Accuracy	Recall	Precision	F1	FPR	FNR
A	psd/beta	0.962	0.947	0.976	0.961	0.023	0.053
A	psd/gamma	0.986	0.975	0.996	0.985	0.004	0.025
A	de/beta	0.981	0.969	0.992	0.980	0.008	0.031
A	de/gamma	0.992	0.984	1	0.992	0	0.016
A	var/beta	0.977	0.966	0.987	0.976	0.013	0.034
A	var/gamma	0.986	0.975	0.996	0.985	0.004	0.025
B	psd/beta	0.973	0.962	0.983	0.972	0.017	0.038
B	psd/gamma	0.990	0.981	0.998	0.989	0.002	0.019
B	de/beta	0.987	0.978	0.996	0.987	0.004	0.022
B	de/gamma	0.993	0.987	0.998	0.992	0.002	0.013
B	var/beta	0.983	0.975	0.990	0.982	0.010	0.025
B	var/gamma	0.992	0.987	0.996	0.991	0.004	0.013
C	psd/beta	0.991	0.991	0.990	0.991	0.01	0.009
C	psd/gamma	0.996	0.991	1	0.995	0	0.009
C	de/beta	0.994	0.991	0.996	0.993	0.004	0.009

C	de/gamma	0.997	0.994	1	0.997	0	0.006
C	var/beta	0.994	0.994	0.994	0.994	0.006	0.006
C	var/gamma	0.995	0.991	0.998	0.994	0.002	0.009

Experimental results demonstrate that all three datasets exhibited significantly superior discriminative performance in the gamma frequency band compared to the beta band. Within the gamma band, differential entropy features demonstrated significantly better classification performance than both power spectral density and variance features, achieving accuracy rates exceeding 99.2%. Following parameter optimization and ten-fold cross-validation, these findings further substantiate the potential predictive power of gamma-band indicators for distinguishing between competent and non-competent groups. Specifically, channels FP1 and P3 consistently outperformed other channels across all three datasets in the gamma band, with the highest-performing channels achieving accuracy rates above 85%, as detailed in the accompanying Table 7.

Table 7. Ten-Fold Cross-Validation Accuracy Rates for Three Feature Types Across Channels in the Gamma Frequency Band.

Feature	Channels	A group Accuracy	B group Accuracy	C group Accuracy
PSD	FP1	55.2500	77.6250	85.2073
	FP2	61.3750	65.1250	66.5427
	O1	68.2500	59.1250	64.4193
	O2	61.6250	63.3750	61.9209
	P3	64.1250	85.6250	79.5759
	P4	53.6250	70.6250	70.4098
	T3	60.5000	59.1250	65.9177
	T4	64.0000	73.5000	66.2848
DE	FP1	71.1250	80.7500	87.2199
	FP2	61.7500	67.5000	63.3054
	O1	62.5000	64.7500	66.0570
	O2	69.8750	64.8750	69.3038
	P3	70.6250	86.3750	81.0775
	P4	60.1250	73.3750	71.1693
	T3	66.3750	62.8750	67.6883
	T4	69.3750	72.5000	65.2832
VAR	FP1	71.1250	80.7500	87.3449
	FP2	62.0000	67.3750	63.4320
	O1	62.7500	64.6250	65.8054
	O2	69.8750	65.0000	69.1772
	P3	70.3750	86.3750	81.0775
	P4	60.1250	73.3750	71.1693
	T3	66.3750	62.8750	67.5633
	T4	69.5000	72.6250	65.2832

5. Dicussion

The current selection process for low-altitude aircraft operators predominantly relies on conventional subjective behavioral observations and psychological scale evaluations, which suffer from limitations such as narrow assessment dimensions and excessive subjectivity. There is an urgent industry need to integrate quantitative objective indicators into talent selection systems. This study designed a novel experimental paradigm where both electroencephalography signals and questionnaire data collected during experiments were utilized for subsequent feature analysis and modeling. Based on resting-state EEG and machine learning approaches, the research identified statistically significant differences in gamma-band differential entropy at the prefrontal FP1 channel

and parietal P3 channel between subjects demonstrating competency and those lacking competency for low-altitude aircraft operation roles, with statistical significance confirmed by t-test results ($p < 0.05$). These findings indicate that the gamma-band DE metric may reflect competency-related variations in attentional resource allocation and information processing efficiency, while simultaneously providing a potential objective physiological marker to supplement existing selection systems primarily dependent on subjective scales and behavioral observations. Considering the operational environment and professional requirements for low-altitude aircraft operators, we hypothesize that the critical competencies determining operational suitability primarily involve attentional allocation capacity and decision-making capability during emergency situations. Although the two significant brain regions identified through EEG analysis govern distinct cognitive functions, their combined activity reflects the essential capabilities of attention distribution and emergency decision-making specifically required for low-altitude aircraft operations. Consequently, for incumbent operators demonstrating insufficient competency, targeted training interventions focusing on these two cognitive domains could enhance their performance to meet operational standards.

From an applied perspective, these findings possess direct implications for education and training programs. First, gamma-band differential entropy values from FP1 and P3 channels could serve as candidate quantitative metrics integrated into selection or training assessment protocols to support decision-making processes or provide objective feedback on training effectiveness. Second, training program development should prioritize targeted exercises for attention maintenance, attentional allocation, emotional regulation during emergencies, and decision-making under unexpected scenarios. Implementation strategies may include graded flight simulation tasks, progressively challenging cognitive load exercises, and scenario-based training paradigms to enhance relevant neural functions. Given the diversity of available training methodologies, after a predetermined training period, short-term neurofeedback or cognitive training could be explored as pilot interventions to evaluate their effects on both the target metric (gamma-band DE) and actual operational performance, thereby identifying optimal training tasks for program optimization.

Nevertheless, this study possesses certain limitations. Constraints related to sample size and experimental equipment indicate several avenues for methodological refinement in future investigations. Primarily, the limited cohort of 20 participants restricts the robustness and generalizability of findings, necessitating larger-scale multi-center replication studies to establish definitive discriminant and application thresholds for this physiological indicator. Furthermore, while the current research exclusively utilized resting-state EEG recordings, the stability of the proposed metric remains unverified under task-performing conditions or simulated operational scenarios. Consequently, subsequent studies should expand sample sizes and incorporate external validation cohorts to verify the discriminant power of gamma-band differential entropy during flight simulations or task-performing conditions. Such investigations should systematically evaluate the correlation between this electrophysiological metric and behavioral measurements, questionnaire scores, and actual training outcomes, while additionally developing multimodal integration models combining EEG, behavioral, and questionnaire data to enhance predictive accuracy and robustness.

In summary, this study methodologically integrates resting-state EEG-derived physiological features with machine learning techniques, providing actionable candidate physiological indicators for objective assessment of low-altitude aircraft operators. The identified biomarkers can be incorporated into selection protocols to enhance objectivity and accuracy in candidate evaluation, thereby reducing resource allocation inefficiencies and subjective biases. Furthermore, training programs can be optimized based on these findings through targeted development of attentional allocation capabilities and emergency decision-making skills. This research demonstrates potential value for improving selection objectivity, enriching competency evaluation dimensions, and informing the design of specialized training interventions.

References

1. Huang, Changqing, Shifeng Fang, Hua Wu, Yong Wang, and Yichen Yang, "Low-altitude intelligent transportation: System architecture, infrastructure, and key technologies," *Journal of Industrial Information Integration*, vol. 42, p. 100694, 2024.
2. Lee, Hai-Wu, and Chi-Shiuan Lee, "Research on logistics of intelligent unmanned aerial vehicle integration system," *Journal of Industrial Information Integration*, vol. 36, p. 100534, 2023.
3. Ebrahim, Yassmin, Brett Molesworth, and Oleksandra Molloy, "Investigating the predictive validity of subjective and objective measures for general aviation pilots' risk propensity," *Safety Science*, vol. 186, p. 106818, 2025.
4. Li, Yuhan, Ke Li, Shaofan Wang, Xiaodan Chen, and Dongsheng Wen, "Pilot behavior recognition based on multi-modality fusion technology using physiological characteristics," *Biosensors*, vol. 12, no. 6, p. 404, 2022.
5. Natheir, Sharif, Sommer Christie, Recai Yilmaz, Alexander Winkler-Schwartz, Khalid Bajunaid, Abdulrahman J. Sabbagh, Penny Werthner, Jawad Fares, Hamed Azarnoush, and Rolando Del Maestro, "Utilizing artificial intelligence and electroencephalography to assess expertise on a simulated neurosurgical task," *Computers in Biology and Medicine*, vol. 152, p. 106286, 2023.
6. Fuentes-Martinez, Victor Juan, Samuel Romero, Miguel Angel Lopez-Gordo, Jesus Minguillon, and Manuel Rodríguez-Álvarez, "Low-cost EEG multi-subject recording platform for the assessment of students' attention and the estimation of academic performance in secondary school," *Sensors*, vol. 23, no. 23, p. 9361, 2023.
7. Aminosharieh Najafi, Taraneh, Antonio Affanni, Roberto Rinaldo, and Pamela Zontone, "Driver attention assessment using physiological measures from EEG, ECG, and EDA signals," *Sensors*, vol. 23, no. 4, p. 2039, 2023.
8. Angkan, Prithila, Behnam Behinaein, Zunayed Mahmud, Anubhav Bhatti, Dirk Rodenburg, Paul Hungler, and Ali Etemad, "Multimodal brain--computer interface for in-vehicle driver cognitive load measurement: Dataset and baselines," *IEEE Transactions on Intelligent Transportation Systems*, vol. 25, no. 6, pp. 5949-5964, 2024.
9. Harel, Asaf, Anna Levkovsky, Idan Nakdimon, Barak Gordon, and Oren Shriki, "EEG-based prediction of reaction time during sleep deprivation," *Sleep*, vol. 48, no. 7, p. zsaf080, 2025.
10. Hu, Haixu, Zhou Fang, Zhiyu Qian, Liuye Yao, Ling Tao, and Bing Qin, "Stress Assessment of Vestibular Endurance Training for Civil Aviation Flight Students Based on EEG," *Frontiers in Human Neuroscience*, vol. 15, p. 582636, 2021.
11. Welch, Peter, "The use of fast Fourier transform for the estimation of power spectra: A method based on time averaging over short, modified periodograms," *IEEE Transactions on audio and electroacoustics*, vol. 15, no. 2, pp. 70-73, 1967.
12. Oppenheim, Alan V., *Discrete-time signal processing*, Pearson Education India, 1999.
13. Treitel, Sven, "Spectral Analysis for Physical Applications: Multitaper and Conventional Univariate Techniques," *American Scientist*, vol. 83, no. 2, pp. 195-197, 1995.
14. Shannon, Claude Elwood, "A mathematical theory of communication," *The Bell system technical journal*, vol. 27, no. 3, pp. 379-423, 1948.
15. Cover, Thomas M., *Elements of information theory*, John Wiley & Sons, 1999.
16. Zheng, Wei-Long, and Bao-Liang Lu, "Investigating critical frequency bands and channels for EEG-based emotion recognition with deep neural networks," *IEEE Transactions on autonomous mental development*, vol. 7, no. 3, pp. 162-175, 2015.
17. Paus, Tomáš, Robert J. Zatorre, Nina Hofle, Zografos Caramanos, Jean Gotman, Michael Petrides, and Alan C. Evans, "Time-related changes in neural systems underlying attention and arousal during the performance of an auditory vigilance task," *Journal of cognitive neuroscience*, vol. 9, no. 3, pp. 392-408, 1997.
18. Corbetta, Maurizio, Gaurav Patel, and Gordon L. Shulman, "The reorienting system of the human brain: from environment to theory of mind," *Neuron*, vol. 58, no. 3, pp. 306-324, 2008.
19. Andersen, Richard A., Lawrence H. Snyder, David C. Bradley, and Jing Xing, "Multimodal representation of space in the posterior parietal cortex and its use in planning movements," *Annual review of neuroscience*, vol. 20, no. 1, pp. 303-330, 1997.
20. Sauseng, Paul, Birgit Griesmayr, Roman Freunberger, and Wolfgang Klimesch, "Control mechanisms in working memory: a possible function of EEG theta oscillations," *Neuroscience & Biobehavioral Reviews*, vol. 34, no. 7, pp. 1015-1022, 2010.